iScience

CellPress

Article

The Input-Output Relationship of AIY Interneurons in *Caenorhabditis elegans* in Noisy Environment

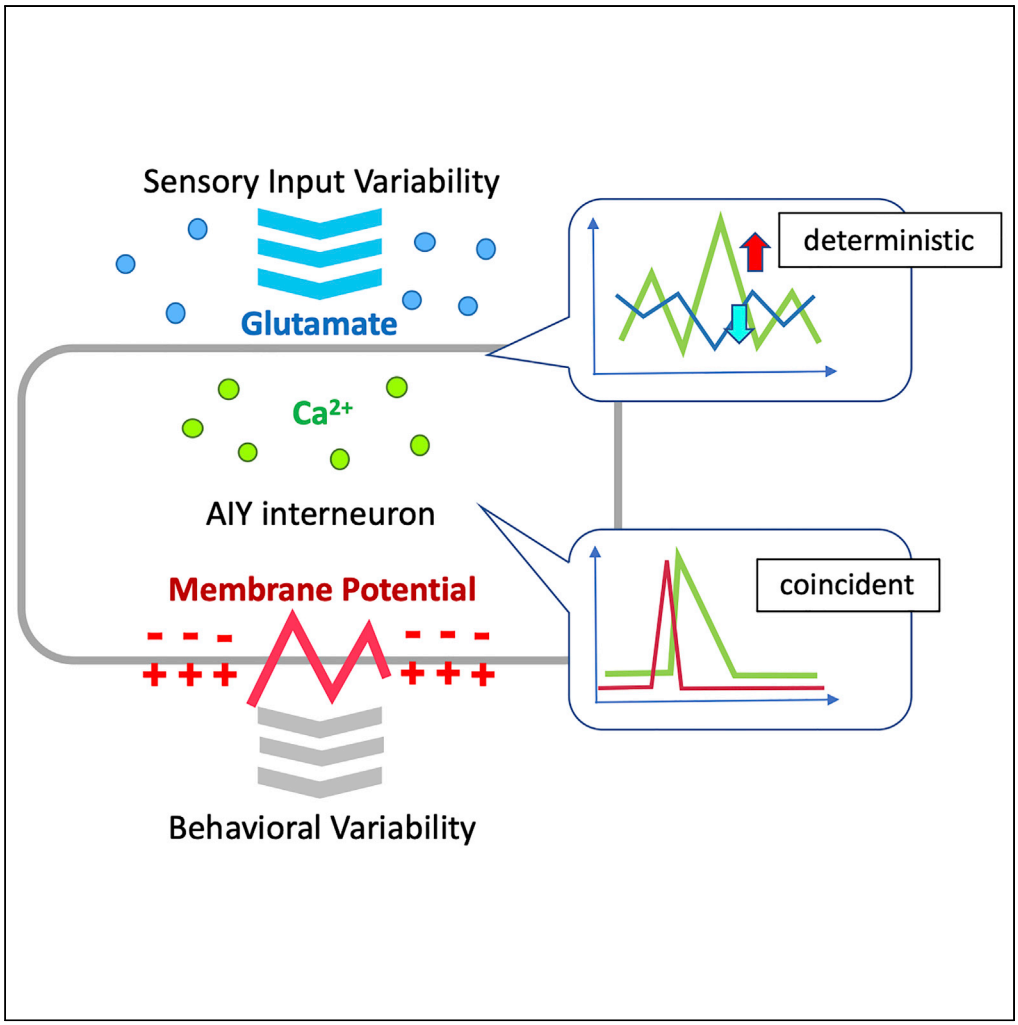

Keita Ashida, Kohji Hotta, Kotaro Oka

oka@bio.keio.ac.jp

HIGHLIGHTS

Glutamate-input fluctuation evokes a sporadic Ca^{2+} response in AIY

The membrane-potential depolarization precedes Ca^{2+} responses in AIY

Ca^{2+} increases in AIY when the glutamate input decreases, and *vice versa*

Mutation of glutamate signaling abolished Ca^{2+} response in AIY

Ashida et al., iScience *19*, 191–203
September 27, 2019
https://doi.org/10.1016/j.isci.2019.07.028

iScience

CellPress

Article

The Input-Output Relationship of AIY Interneurons in *Caenorhabditis elegans* in Noisy Environment

Keita Ashida,[1] Kohji Hotta,[1] and Kotaro Oka[1,2,3,4,*]

SUMMARY

Determining how neurotransmitter input causes various neuronal activities is crucial to understanding neuronal information processing. In *Caenorhabditis elegans*, AIY interneurons receive several sources of sensory information as glutamate inputs and regulate behavior by integrating these inputs. However, the relationship between glutamate input and the Ca^{2+} response in AIY under environmental noise, in other words, without explicit stimulation, remains unknown. Here, we show that glutamate-input fluctuations evoke a sporadic Ca^{2+} response in AIY without stimulation. To ensure that Ca^{2+} response can be considered AIY output, we show that the membrane-potential depolarization precedes Ca^{2+} responses in AIY. We used an odor as model stimulation to modulate the sensory inputs. Simultaneous imaging of glutamate input and Ca^{2+} response, together with glutamate transmission mutants, showed that glutamate-input fluctuations evoke sporadic Ca^{2+} responses. We identified the input-output relationships under environmental noise *in vivo*, and our results address the relationship between sensory-input fluctuations and behavioral variability.

INTRODUCTION

Information processing from sensory inputs to regulate behavior in noisy environments is a fundamental topic in neuroscience. To improve our understanding of such information processing, the relationship between the noise level of the stimulation and animal perception has been studied in depth (Faisal et al., 2008; Nienborg and Cumming, 2009; Renart and Machens, 2014). However, at the neuronal level these relationships remain largely unclear. Although the input-output relationship in neurons has also been thoroughly investigated (Augustine et al., 2003; Cichon and Gan, 2015; Destexhe, 2011; Frick et al., 2004; Losonczy et al., 2008; Ogawa and Oka, 2015; Stuart and Spruston, 2015), it remains unknown how neurotransmitter inputs affect postsynaptic neuronal activity *in vivo* in noisy environments, because simultaneous measurement of input and output *in vivo* is technically difficult due to the complexity of the networks involved (Ogawa and Oka, 2015; Prešern et al., 2015; Stuart and Spruston, 2015).

The nematode *Caenorhabditis elegans* is a suitable model for investigating this question. It has a simple neuronal circuit (White et al., 1986), as well as optical transparency, making it well suited for visualization with various imaging techniques (Kerr and Schafer, 2006). The AIY interneurons of *C. elegans* are particularly suitable for this purpose; they receive various sensory inputs, including gustatory, olfactory, and thermal information (Chalasani et al., 2007; Clark et al., 2006; Satoh et al., 2014), which regulate the animal's behavior following integration (Kocabas et al., 2012; Li et al., 2014; Satoh et al., 2014). Furthermore, AIY interneurons show a sporadic Ca^{2+} response regardless of the presence of explicit stimulation (Chalasani et al., 2007; Clark et al., 2006), whereas sensory neurons show a deterministic Ca^{2+} response to environmental stimulation (Chalasani et al., 2007; Clark et al., 2006; Kato et al., 2014; Tsukada et al., 2016). Both glutamate receptor mutations and the ablation of sensory neurons have been shown to abolish the Ca^{2+} response to sensory stimulation in AIY (Chalasani et al., 2007; Clark et al., 2006). This suggests that glutamate input to AIY can evoke the sporadic Ca^{2+} response as a result of sensory input integration under natural noise.

We used several simultaneous fluorescence imaging techniques to identify the input-output relationship in AIY in a noisy environment *in vivo*. To ensure that Ca^{2+} spikes could be considered AIY output, we first showed that depolarization of the membrane potential precedes Ca^{2+} spikes, by simultaneously imaging both in AIY. We used an odor, isoamyl alcohol (IAA) as model stimulation to modulate the sensory inputs, and simultaneous imaging of glutamate input and the Ca^{2+} response showed that glutamate input decreases when the Ca^{2+} spikes occur, with or without odor stimulation, and *vice versa*. We also investigated these relationships in both the glutamate receptor and glutamate-defective mutants and showed that

[1]Department of Biosciences and Informatics, Faculty of Science and Technology, Keio University, Yokohama 223-8522, Japan

[2]Graduate Institute of Medicine, College of Medicine, Kaohsiung Medical University, Kaohsiung City 80708, Taiwan

[3]Waseda Research Institute for Science and Engineering, Waseda University, 2-2 Wakamatsucho, Shinjuku, Tokyo 162-8480, Japan

[4]Lead Contact

*Correspondence: oka@bio.keio.ac.jp

https://doi.org/10.1016/j.isci.2019.07.028

fluctuations in glutamate input evoke the sporadic Ca^{2+} response in AIY. As far as we know, this is the first report identifying the input-output relationship for fluctuations under natural environmental noise *in vivo*. Glutamate inputs represent sensory inputs, and AIY neurons have been reported to regulate behavior; our results thus suggest that fluctuation in sensory input induces behavioral variability.

RESULTS

Membrane-Potential Spike Precedes Ca^{2+} Response in AIY

To quantify the input-output relationship in a single neuron *in vivo*, we investigated AIY interneurons in *C. elegans*. AIY neurons receive environmental information from sensory neurons via glutamate as a neurotransmitter and show a large sporadic Ca^{2+} response (hereafter, a "spike") as a result of sensory integration (Chalasani et al., 2007; Clark et al., 2006). In *C. elegans*, Ca^{2+} is thought to be the main charge carrier in membrane-potential changes, due to the lack of voltage-gated Na^{+} channels in its neurons (Faumont et al., 2011, 2006; Gao and Zhen, 2011; Goodman et al., 1998; Mellem et al., 2008; Shidara et al., 2013). Recently, the relationship between membrane potential and Ca^{2+} channels has been thoroughly investigated, and it has been shown that Ca^{2+} channels are necessary for membrane-potential spikes (Liu et al., 2018; Shindou et al., 2019). Ca^{2+} responses in AIY regulate the animal's behavior (Li et al., 2014), so the results of information processing should be expressed as membrane-potential changes. However, the relationship between Ca^{2+} and membrane potential in AIY remains unclear (Liu et al., 2018, 2009; Shidara et al., 2013), because it has not been measured simultaneously in AIY. We therefore measured both simultaneously, using a genetically encoded voltage indicator, ArcLight (Jin et al., 2012), and a genetically encoded Ca^{2+} indicator, R-GECO (Zhao et al., 2011) (Figure 1A). As previously suggested (Faumont et al., 2012), changes in membrane potential appeared as a spike-like response under ArcLight fluorescence, similar to a Ca^{2+} spike (Figure 1B). Importantly, these membrane-potential spikes were coincident with Ca^{2+} spikes. Membrane-potential changes were detected at the neurite and even at the soma, as reported in our earlier study (Shidara et al., 2013).

To investigate the relationship between membrane-potential spikes and Ca^{2+} spikes, we collected and summarized the data (Figure 1C). Membrane-potential spikes preceded Ca^{2+} spikes, and their amplitudes were not modulated by odor presentation (Figure 1D). However, the amplitudes of Ca^{2+} spikes and membrane-potential spikes were not correlated (Figure 1E). Based on these results, membrane-potential changes precede Ca^{2+} changes. In subsequent analyses, therefore, we consider Ca^{2+} spikes to be AIY output.

Glutamate Input and Ca^{2+} Response to Odor Stimulation in AIY Interneurons

In AIY interneurons, glutamate input reflects environmental information from sensory neurons, and sporadic Ca^{2+} spikes occur as a result of sensory integration (Chalasani et al., 2007; Clark et al., 2006). These glutamate inputs emanate from gustatory, olfactory, and thermal sensory neurons (Chalasani et al., 2007; Clark et al., 2006; Satoh et al., 2014; White et al., 1986); therefore, in the absence of explicit changes of stimulation, glutamate inputs to AIY presumably reflect environmental noise, such as fluctuations in environmental factors such as temperature, local salt concentration, and olfactory molecules. AIY neurons receive inhibitory glutamate inputs via a glutamate-gated chloride channel, GLC-3 (Clark et al., 2006; Horoszok et al., 2001; Serrano-Saiz et al., 2013). AIY neurons exhibit Ca^{2+} spikes in response to odor stimulation because sensory neurons reduce their Ca^{2+} response and neurotransmitter release upon addition of odor (Chalasani et al., 2007; Ventimiglia and Bargmann, 2017) (Figure S1). Mutation of *glc-3* or glutamate transmission abolishes Ca^{2+} spikes in response to odor in AIY neurons (Chalasani et al., 2007). Therefore, sporadic Ca^{2+} spikes in AIY could occur in response to variable glutamatergic inputs representing environmental noise. To demonstrate this directly, we simultaneously measured glutamatergic inputs and Ca^{2+} responses in AIY interneurons, using a genetically encoded glutamate indicator, iGluSnFR (Marvin et al., 2013), and a genetically encoded Ca^{2+} indicator, R-GECO (Zhao et al., 2011), respectively (Figure 2A).

As a previous study hypothesized that odor (IAA) stimulation could modify glutamate input to AIY (Chalasani et al., 2007), we selected IAA as model sensory stimulation. We measured glutamate input and the Ca^{2+} response with and without odor stimulation (Figure 2B). The glutamate input to AIY decreased following odor application and transiently increased following odor removal, in a deterministic manner (Figure 2C). These responses to odor correspond to the responses of sensory neurons (Chalasani et al., 2007; Shidara et al., 2017). Although there were deterministic changes in glutamate input, large Ca^{2+} spikes were observed even without odor, and often at the onset of odor stimulation, as reported previously (Chalasani et al., 2007). Odor application typically evoked Ca^{2+} spikes immediately in wild-type animals (see N2

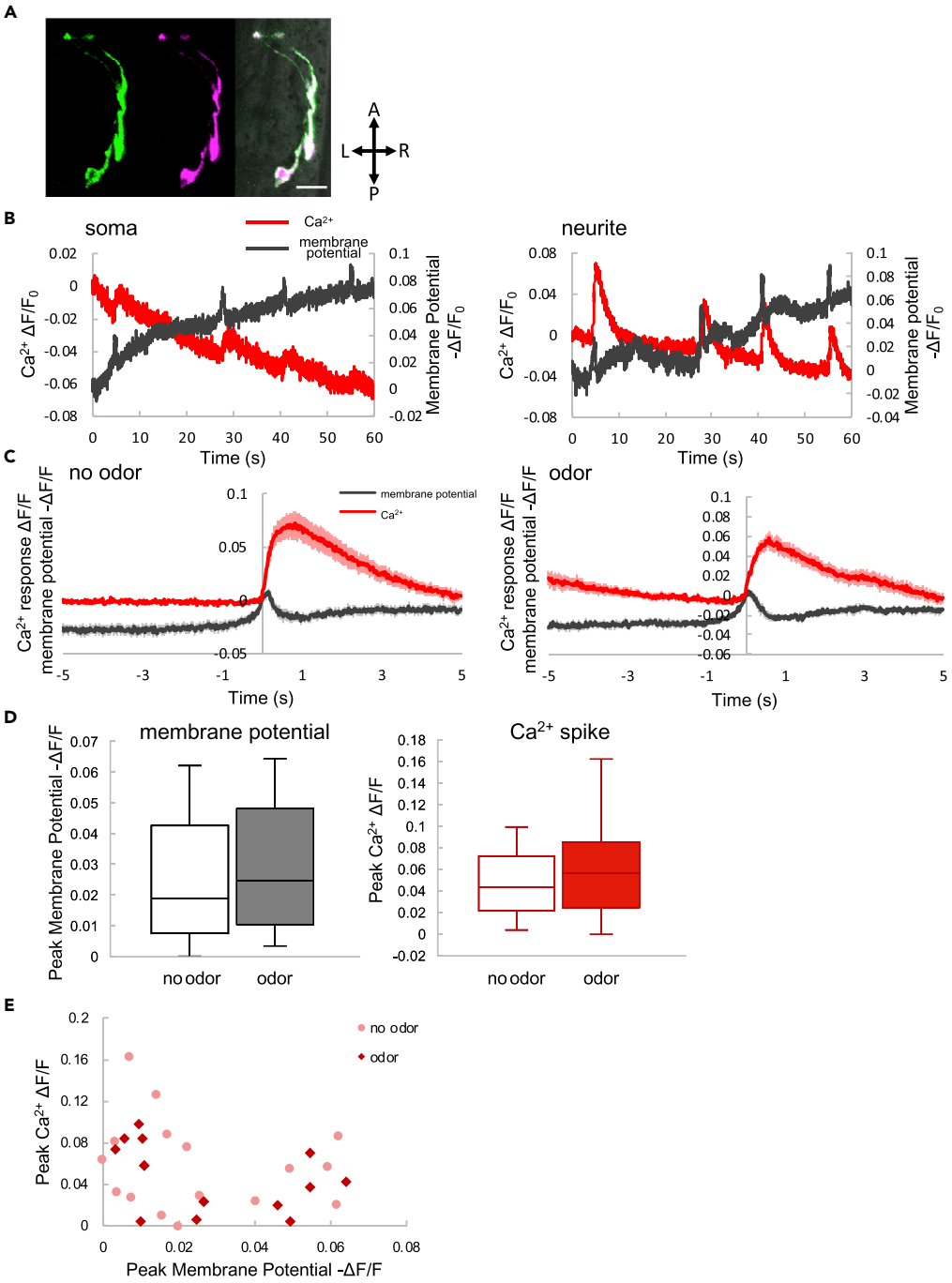

Figure 1. Simultaneous Imaging of Membrane Potential and Ca^{2+} in AIY Interneurons

(A) Confocal image of the voltage indicator (ArcLight: green, left) and Ca^{2+} indicator (R-GECO magenta, middle). The merged image is on the right. Scale bar, 10 μm. A, anterior; L, left; P, posterior; R, right.

(B) Representative results of Ca^{2+} (red) and membrane potentials (black) at the soma (left) and neurite (right).

(C) Averaged Ca^{2+} spike (red) and membrane-potential spike (black) without (left) and with (right) odor. The shadows around the solid lines indicate the standard error of the mean (SEM) (no odor, N = 20, n = 16; odor, N = 10, n = 15).

(D) Membrane potential (left) and Ca^{2+} spike (right) intensities, with (filled boxes) and without (hollow boxes) odor. Box plots include the median (center line), quartiles (boxes), and range (whiskers). The statistical metrics are as follows: membrane potential, p = 0.38; Ca^{2+}, p = 0.85; paired t tests (no odor, N = 20, n = 16; odor, N = 10, n = 15).

Figure 1. *Continued*

(E) Correlation between Ca^{2+} spike amplitude and membrane-potential spike amplitude. The red diamonds and pink dots are the responses in the presence and absence of odor stimulation, respectively. The statistical metrics are as follows: no odor, Pearson correlation coefficient (PCC) = −0.19, p = 0.48; odor, PCC = −0.40, p = 0.14 (no odor, N = 20, n = 16; odor, N = 10, n = 15).

in Figure 6C), suggesting that glutamate decreases, induced by odor application, evoke Ca^{2+} spikes. Moreover, odor presence increased the frequency of Ca^{2+} spikes (see N2 in Figure 6D). This suggests that reducing glutamate input via odor application causes Ca^{2+} spikes.

Glutamatergic Input Decreases when the Ca^{2+} Response Increases in AIY under Natural Noise, and *Vice Versa*

When quantifying the average response of glutamatergic input and Ca^{2+} in AIY to odor, we found that decreases in glutamatergic input appeared to be related to Ca^{2+} spikes (Figure 3A). To investigate this

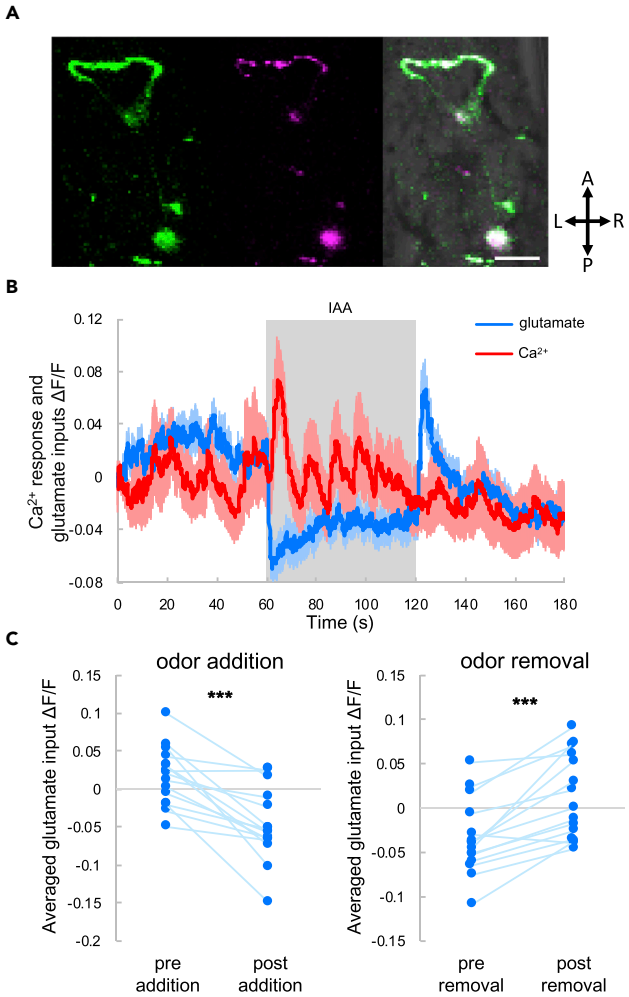

Figure 2. Simultaneous Imaging of Glutamate Inputs and Ca^{2+} Responses in AIY Interneurons

(A) Confocal image of the glutamate indicator (iGluSnFR: green, left) and Ca^{2+} indicator (R-GECO: magenta, middle) in AIY. The merged image is on the right. Scale bar, 10 μm. A, anterior; L, left; P, posterior; R, right.

(B) Averaged glutamate input (blue) and Ca^{2+} response (red) to odor. The shaded region indicates isoamyl alcohol (IAA) stimulation, and the shadows around the solid lines indicate the SEM.

(C) Averaged glutamate intensities before (pre-addition) and after (post-addition) odor addition (left). Glutamate intensities before (pre-removal) and after (post-removal) odor stimulation removal (right). The statistical metrics are as follows: left, p = 0.00010; right, p = 0.000086; paired t test (N = 15). ***p < 0.001.

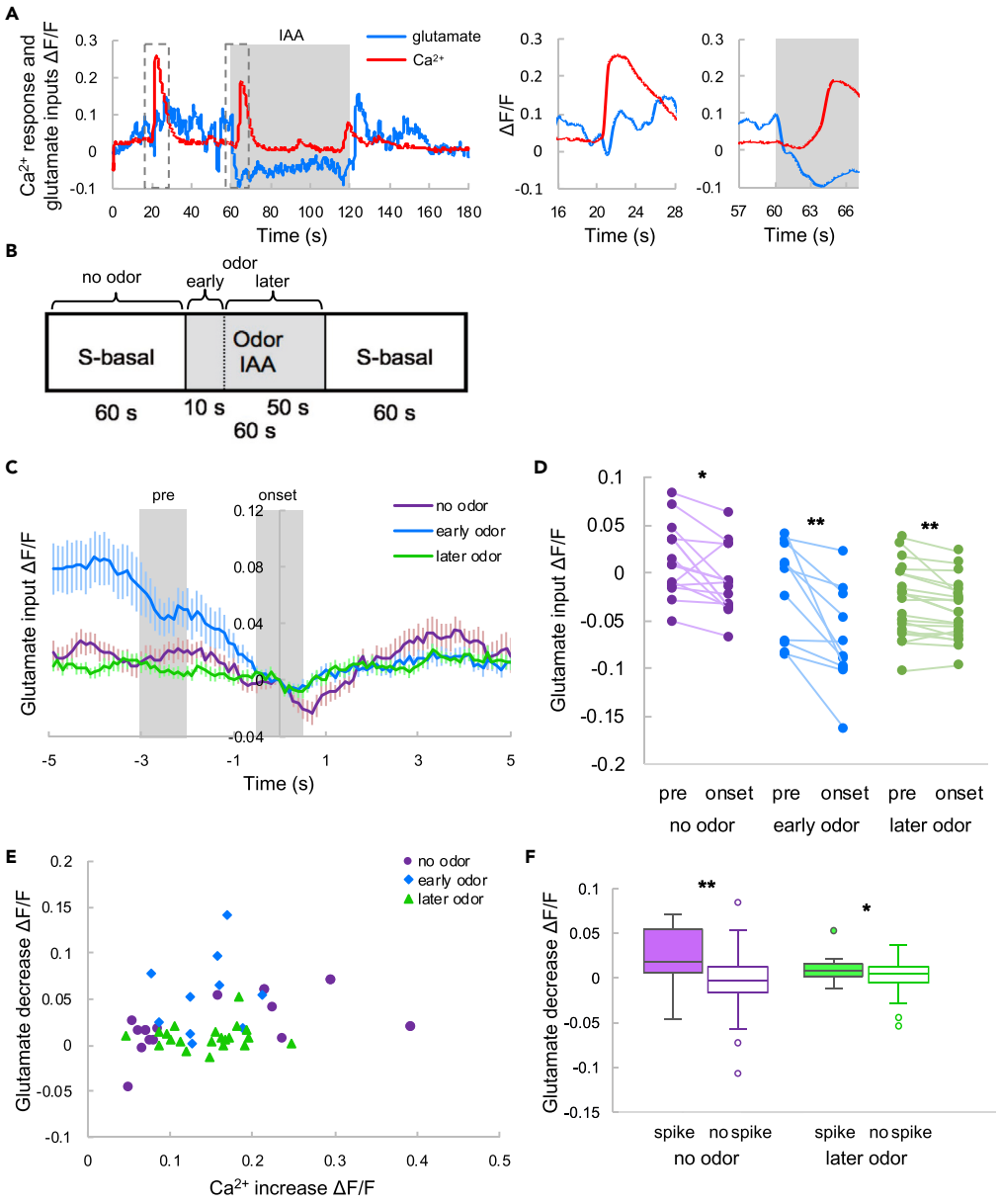

Figure 3. Glutamate Input When the Ca^{2+} Spike Occurs

(A) Representative responses of Ca^{2+} and glutamate input (left). Magnifications of the dotted boxes showing the responses without (middle) and with (right) odor stimulation. The blue and red lines are the glutamate input and Ca^{2+} response, respectively. The shaded region indicates IAA stimulation.

(B) Definition of the response categories.

(C) The averaged glutamate responses coincident with Ca^{2+} spikes. Time 0 indicates the onset of Ca^{2+} spikes. All glutamate responses were normalized to zero at time 0. The purple, blue, and green lines indicate the responses under the no odor, early odor, and later odor conditions, respectively (defined in B). The error bars indicate the SEM (N = 15; no odor, n = 15; early odor, n = 11; later odor, n = 21).

(D) Glutamate inputs before the Ca^{2+} spike and at spike onset. "Pre" indicates the average intensity from −3 to −2 s in (C), and "onset" indicates the average intensity from −0.5 to +0.5 s. The statistical metrics are as follows: no odor, p = 0.010; early odor, p = 0.0024; later odor, p = 0.0037; paired t test (N = 15; no odor, n = 15; early odor, n = 11; later odor, n = 21). *p < 0.05, **p < 0.01.

(E) Correlation between glutamate decreases and Ca^{2+} increases. The purple dots, blue diamonds, and green triangles are correlations under the no odor, early odor, and later odor conditions, respectively. The statistical metrics are as

Figure 3. *Continued*

follows: no odor, PCC = 0.58, p = 0.022; early odor, PCC = 0.080, p = 0.81; later odor, PCC = 0.069, p = 0.77 (no odor, n = 15; early odor, n = 11; later odor, n = 21).

(F) Glutamate decreases with and without Ca^{2+} spikes. The filled and hollow box plots indicate decreases with and without a spike, respectively. Box plots indicate the median (center line), quartiles (boxes), and range (whiskers). The statistical metrics are as follows: no odor, p = 0.0062; later odor, p = 0.037; Welch's t test (N = 15; no odor, spike, n = 15; no odor, no spike: n = 89; later odor, spike, n = 21; later odor, no spike, n = 69) *p < 0.05, **p < 0.01.

relationship further, we classified conditions into three categories: no odor, early odor, and later odor (Figure 3B); glutamatergic inputs were collected and aligned with the timing of Ca^{2+} spikes (Figure 3C). Glutamatergic inputs decreased before the Ca^{2+} spikes, regardless of odor presentation (Figure 3D). Decreasing levels of glutamate did not show a strong correlation with Ca^{2+} spike amplitude (Figure 3E) in any of the three conditions. These results imply that decreases in glutamatergic inputs are necessary to trigger Ca^{2+} spikes. We also compared the extent of glutamate decreases in the presence or absence of Ca^{2+} spikes (Figure 3F) and found that glutamate input decreased significantly when Ca^{2+} spikes occurred, with or without odor, which suggests that decreases in glutamate evoke Ca^{2+} spikes.

To support the idea that decreases in glutamate induce a Ca^{2+} response, we investigated whether Ca^{2+} increases when glutamate decreases. We collected and aligned Ca^{2+} traces with the timing of decreases in glutamatergic inputs (Figure 4A) and found that Ca^{2+} reliably increases when glutamatergic input decreases, with or without odor (Figure 4B). Moreover, the degree of increase was significantly larger than in the randomly resampled data (Figures 4C and 4D). These findings show that Ca^{2+} increases when glutamate decreases and support the idea that decreases in glutamate induce a Ca^{2+} response.

The GLC-3 Receptor Primarily Mediates a Sporadic Ca^{2+} Response in AIY under Odor Stimulation

We demonstrated that glutamate decreases when Ca^{2+} increases, and *vice versa*. Previous research suggests that the glutamate-gated chloride channel, GLC-3, is crucial for the sensory-input-evoked Ca^{2+} response in AIY (Aoki et al., 2017; Chalasani et al., 2007; Horoszok et al., 2001; Ohnishi et al., 2011). Therefore, we investigated the relationship between Ca^{2+} and glutamate input in a *glc-3* mutant. We detected the same type of changes in glutamate input following odor stimulation in *glc-3* mutants as in wild-type (N2) animals (Figures 5A and 5B), and found that GLC-3 mutation had a limited effect on the Ca^{2+} response evoked by odor application (see *glc-3* in Figure 6C). However, the Ca^{2+} spike frequency decreased significantly compared with N2, both with and without odor stimulation (see *glc-3* in Figure 6D). Next, glutamatergic inputs were collected and aligned with the timing of Ca^{2+} spikes, as was done for the N2 animals (Figure 5C). Glutamate decreases were abolished under odor stimulation, but not in the absence of odor stimulation (Figure 5D). The extent of the decrease when accompanied by a Ca^{2+} spike was not significantly different from that without a Ca^{2+} spike under the odor stimulation, but was significantly larger in the absence of odor stimulation (Figure 5E). AIY neurons have a metabotropic glutamate receptor, MGL-1 (Jeong and Paik, 2017; Kang and Avery, 2009), which could play a role in initiating Ca^{2+} spikes. These results suggest that fluctuations in glutamate input via the GLC-3 receptor are important for the sporadic Ca^{2+} spikes.

Glutamate Input Evokes a Sporadic Ca^{2+} Response in AIY

We thus showed that the GLC-3 receptor plays a crucial role in the sporadic Ca^{2+} spikes. We used a glutamate-defective mutant, *eat-4*, to directly reveal the effect of glutamate input on AIY. EAT-4 is a vesicular glutamate transporter, and *eat-4* mutants are defective in glutamate transmission (Chalasani et al., 2007; Lee et al., 1999). In contrast to the N2 animals and *glc-3* mutants, the glutamate response following odor application and removal was abolished (Figures 6A and 6B). Moreover, the Ca^{2+} response to odor stimulation was also abolished (Figure 6C), and in fact the Ca^{2+} spike rarely occurred at all, with or without odor stimulation (Figure 6D). We collected and aligned glutamate input with the timing of Ca^{2+} spike initiation (Figure 6E), but no decreases were observed (Figure 6F), and the extent of decrease in the presence of a Ca^{2+} spike did not differ from that without a Ca^{2+} spike (Figure 6G). These results show that glutamate-input fluctuations evoke sporadic Ca^{2+} spikes in AIY neurons.

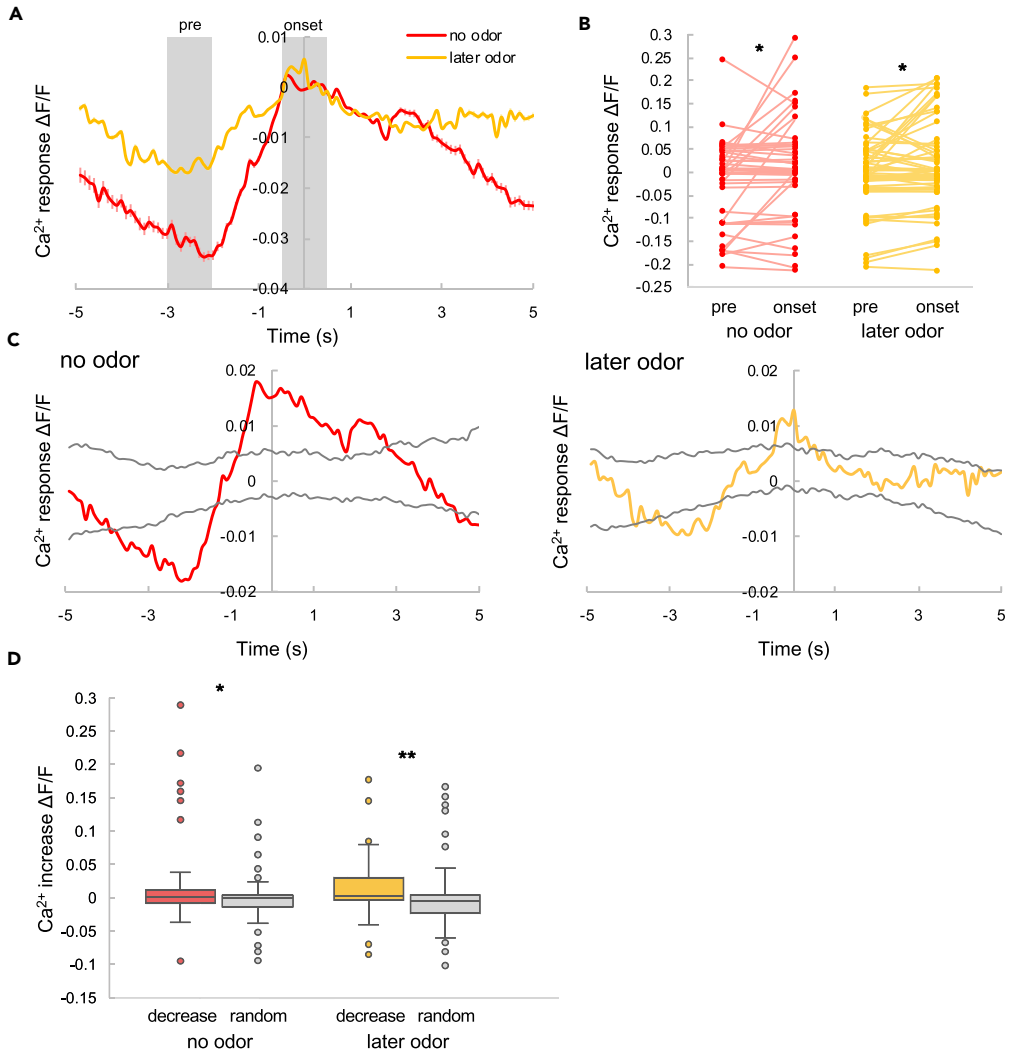

Figure 4. Ca^{2+} Response to Decreases in Glutamate Input

(A) Ca^{2+} response to decreases in glutamate input. Time 0 indicates the time when the glutamate decreases. All Ca^{2+} responses were normalized to zero at time 0. The red and yellow lines indicate the response under the no odor and later odor conditions, respectively. The shadows indicate the SEM (for the Ca^{2+} response under later odor condition, the shadows are too small to see; N = 15; no odor, n = 43; later odor, n = 61).

(B) Ca^{2+} intensities before ("pre"; averaged from −3 to −2 s in A) and after ("onset"; averaged from −0.5 to +0.5 s in A) glutamate decrease. The statistical metrics are as follows: no odor, p = 0.014; later odor, p = 0.014; paired t test (N = 15; no odor, n = 43; later odor, n = 61). *p < 0.05.

(C) Ca^{2+} responses to decreases in glutamate input relative to randomly selected data with (right) and without odor (left). The gray lines indicate the averaged randomly selected data ± 3 SD (see Methods).

(D) Ca^{2+} increases with glutamate decreases (colored boxes) and by random selection (gray boxes). Box plots indicate the median (center line), quartiles (boxes), and range (whiskers). The statistical metrics are as follows: no odor, p = 0.045; later odor, p = 0.0015. Wilcoxon rank-sum test (N = 15; no odor, decrease, n = 43; no odor, random, n = 100; later odor, decrease, n = 61; later odor, random, n = 100). *p < 0.05, **p < 0.01.

DISCUSSION

In this article, we present two sets of simultaneous imaging investigations into the effects of environmental fluctuations on the interaction between Ca^{2+} and membrane potentials and Ca^{2+} and neurotransmitter (glutamate) inputs in AIY interneurons. By combining this approach with the use of mutant strains, we succeeded in determining the input-output relationship. We showed that membrane-potential spikes precede Ca^{2+} spikes in AIY, a previously unknown relationship. Moreover, decreases

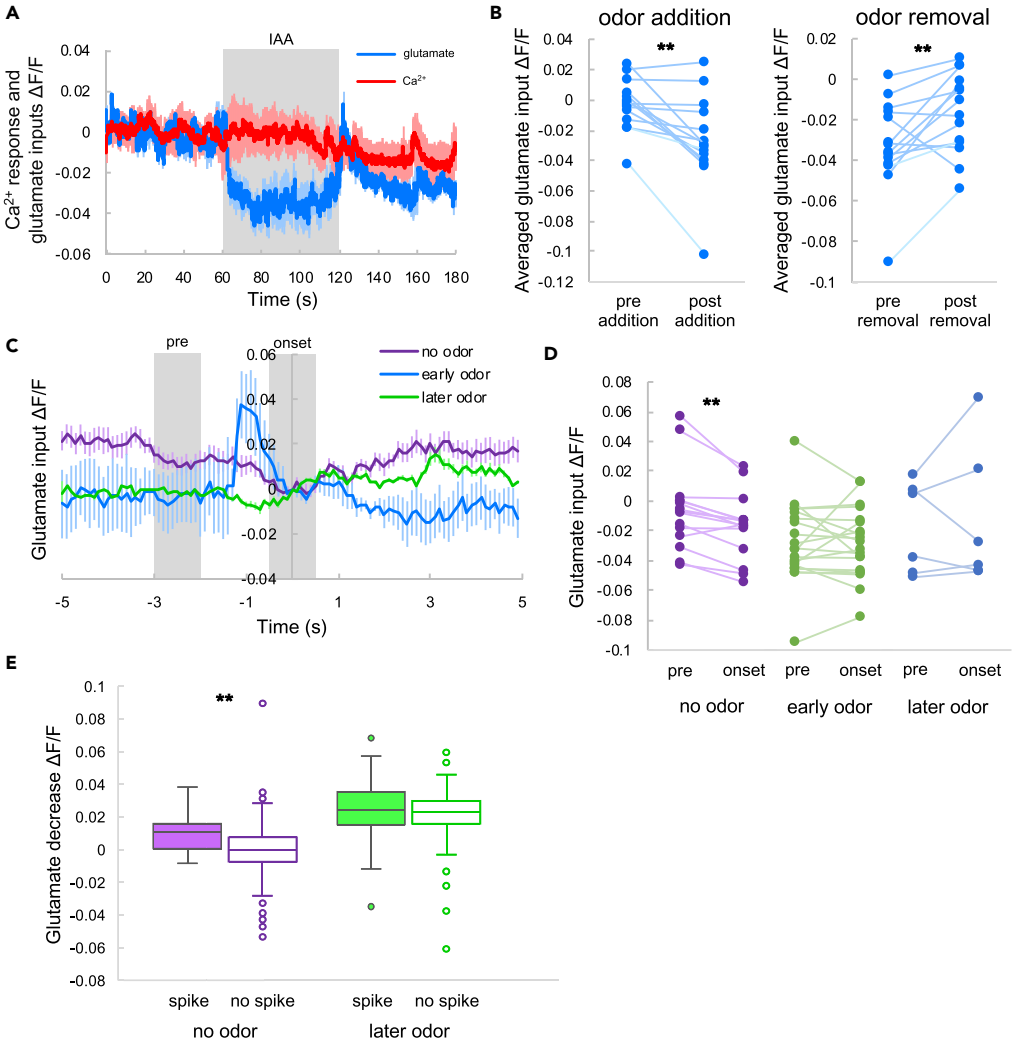

Figure 5. Ca^{2+} Responses and Glutamate Inputs in *glc-3* Mutants

(A) Averaged glutamate inputs (blue) and Ca^{2+} responses (red) to odor. The shaded region indicates IAA stimulation, and the shadows around the solid lines indicate the SEM (N = 12).

(B) Glutamate intensities before (pre-addition) and after (post-addition) odor stimulation onset (left), and average intensities before (pre-removal) and after (post-removal) odor stimulation removal (right). The statistical metrics are as follows: left, p = 0.0030; right, p = 0.0018; paired t test (N = 12). **p < 0.01.

(C) Averaged glutamate responses coincident with Ca^{2+} spikes. Time 0 indicates the onset of Ca^{2+} spikes. All glutamate responses were normalized to zero at time 0. The purple, blue, and green lines indicate the responses under the no odor, early odor, and later odor conditions, respectively. Shadows indicate the SEM (N = 12, no odor, n = 15; early odor, n = 6; later odor, n = 20).

(D) Glutamate input before the Ca^{2+} spike and at spike onset. "Pre" indicates the average intensity from −3 to −2 s in (C), and "onset" indicates the average intensity from −0.5 to +0.5 s. The statistical metrics are as follows: no odor, p = 0.0012; early odor, p = 0.65; later odor, p = 0.89; paired t test (N = 12, no odor, n = 15; early odor, n = 6; later odor, n = 20). **p < 0.01.

(E) Averaged glutamate decreases with (filled boxes) and without (hollow boxes) Ca^{2+} spikes. Box plots indicate the median (center line), quartiles (boxes), and range (whiskers). The statistical metrics are as follows: no odor, p = 0.0027; later odor, p = 0.58; Welch's t test (N = 12, no odor, spike, n = 15; no odor, no spike, n = 114; later odor, spike, n = 20; later odor, no spike, n = 82). **p < 0.01.

in glutamate in response to environmental fluctuations evoke sporadic Ca^{2+} spikes. We thus succeeded, for the first time, in identifying the relationship between input and output fluctuations in response to environmental fluctuations *in vivo*.

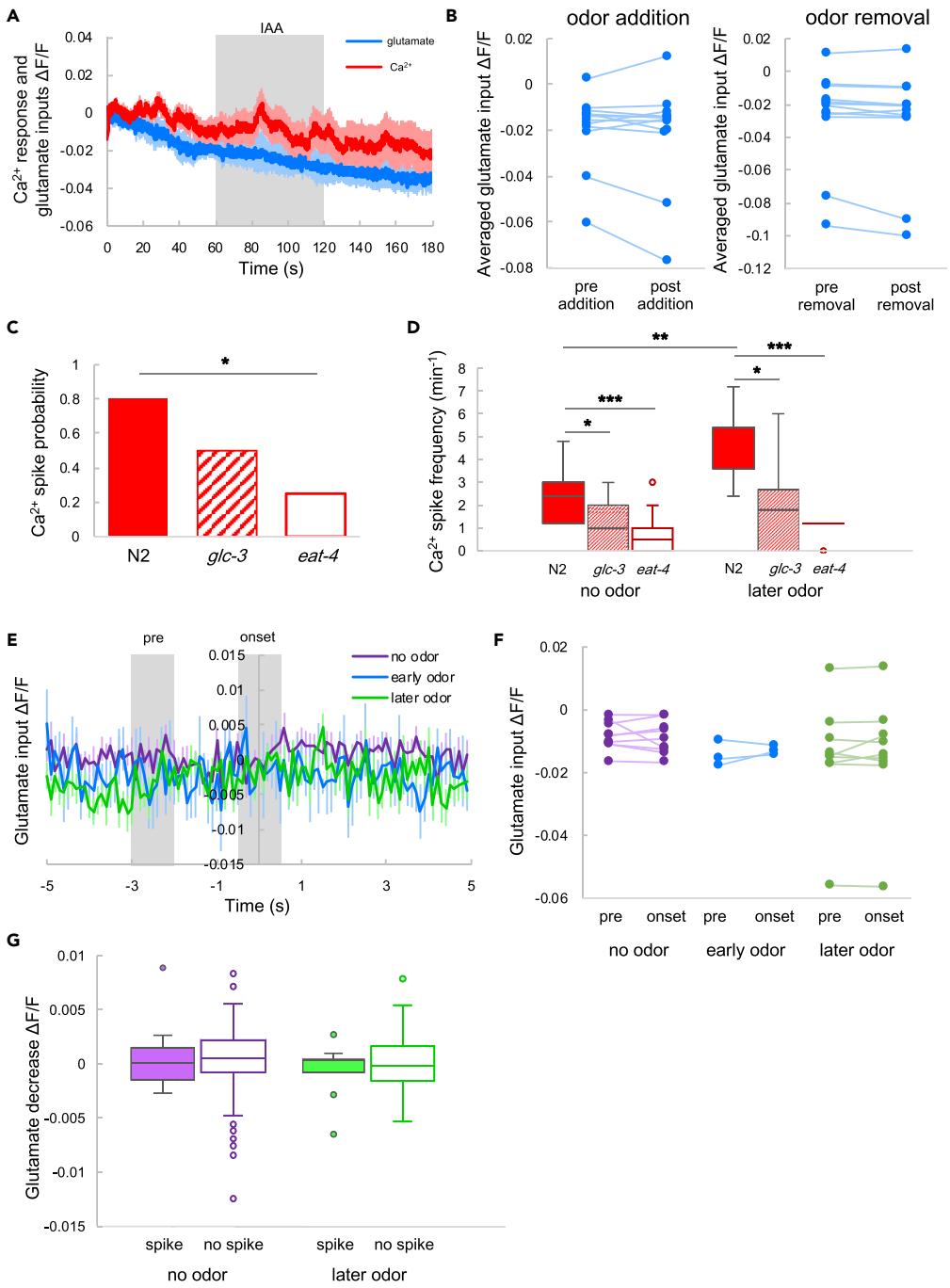

Figure 6. Ca^{2+} Responses and Glutamate Inputs in *eat-4* Mutants

(A) Averaged glutamate input (blue) and Ca^{2+} response (red) to odor. The shaded region indicates IAA stimulation and the shadows around the solid lines indicate the SEM (N = 12).

(B) Average glutamate intensity before (pre-addition) and after (post-addition) odor stimulation onset (left), and average intensity before (pre-removal) and after (post-removal) odor stimulation removal (right). Error bars indicate the SEM. The statistical metrics are as follows: left, p = 0.41; right, p = 0.055; paired t test (N = 12).

(C) Ca^{2+} spike probability following odor addition. Comparison between N2 animals and *glc-3* mutants: p = 0.13; comparison between N2 animals and *eat-4* mutants: p = 0.014. Fisher's exact test with Holm correction (N2, N = 15; *glc-3*, N = 12; *eat-4*, N = 12); *p < 0.05.

(D) Ca^{2+} spike frequency in N2 (filled), *glc-3* (striped), and *eat-4* mutants (hollow) with and without odor. Box plots indicate the median (center line), quartiles (boxes), and range (whiskers). The statistical metrics are as follows: N2 data comparison

Figure 6. *Continued*

between no odor and later odor, p = 0.0045; *glc-3* data comparison between no odor and later odor, p = 0.34; *eat-4* data comparison between no odor and later odor, p = 0.34; Wilcoxon signed rank test. No odor data comparison between N2 and *glc-3*, p = 0.024; no odor data comparison between N2 and *eat-4*, p = 0.00044; later odor data comparison between N2 and *glc-3*, p = 0.014; later odor data comparison between N2 and *eat-4*, p = 0.000015; Wilcoxon rank-sum test. The Holm method was used for the correction (N2, N = 15; *glc-3*, N = 12; *eat-4*, N = 12). *p < 0.05, **p < 0.01, ***p < 0.001.

(E) Averaged glutamate responses coincident with Ca^{2+} spikes. Time 0 indicates the onset of the Ca^{2+} spike. All glutamate responses were normalized to zero at time 0. The purple, blue, and green lines indicate the responses under the no odor, early odor, and later odor conditions, respectively. The bars indicate the SEM (N = 12, no odor: n = 9; early odor, n = 3; later odor, n = 9).

(F) Glutamate input before Ca^{2+} spikes and at Ca^{2+} spike onset. "Pre" indicates the average intensity from −3 to −2 s in (E), and "onset" indicates the average intensity from −0.5 to +0.5 s. The statistical metrics are as follows: no odor: p = 0.60; early odor, p = 0.53; later odor, p = 0.50; paired t test (N = 12; no odor, n = 9; early odor, n = 3; later odor, n = 9).

(G) Averaged glutamate decreases (filled boxes) with and without (hollow boxes) Ca^{2+} spikes. Box plots indicate the median (center line), quartiles (boxes), and range (whiskers). The statistical metrics are as follows: no odor, p = 0.88; later odor, p = 0.48; Welch's t test (N = 12, no odor, spike, n = 9; no odor, no spike, n = 108; later odor, spike, n = 9; later odor, no spike, n = 100).

Glutamate inputs to AIY represent sensory neuronal outputs (Chalasani et al., 2007; Serrano-Saiz et al., 2013; White et al., 1986), and Ca^{2+} responses in AIY correlate with velocity and turn behavior (Li et al., 2014). Therefore, our results suggest that fluctuations in sensory input induce behavioral variability. It is difficult to address the relationship between sensory input and behaviors under environmental noise, because of the low signal-to-noise ratio (Faumont et al., 2012). Our results thus provide novel insights into the relationship between sensory-input fluctuation and behavioral variability.

In previous research, noise has been applied artificially (Nienborg and Cumming, 2009; Renart and Machens, 2014) and is thus not reflective of real environmental fluctuation. Controlling noise is an appropriate strategy for understanding perception, but it is not suitable for evaluating spontaneous variability. Here, we showed that Ca^{2+} spikes are caused by glutamate-input fluctuations. AIY neurons play an important role in sensory integration (Chalasani et al., 2007; Clark et al., 2006; Yoshida et al., 2012) and regulate behavior, and Ca^{2+} responses are correlated with reversal behavior and locomotion speed (Kocabas et al., 2012; Li et al., 2014). Therefore, changing behaviors under natural conditions are presumably caused by fluctuations in sensory input under environmental noise. Our approach of evaluating the input-output relationship in AIY under environmental fluctuations aids understanding of resting-state dynamics in complex neural circuits.

We identified the relationship between neurotransmitter inputs and the Ca^{2+} response. In previous research (Branco and Häusser, 2010; Callaway and Katz, 1993; Kramer et al., 2013), caged compounds and the stimulation of presynaptic neurons were used to investigate these relationships. However, such stimulation is often intense and artificial, and neurotransmitter inputs are not directly measurable. To address these shortcomings, we first demonstrated the relationship between neurotransmitter inputs and Ca^{2+} responses under naturally occurring physiological conditions, and then quantified the input-output relationships using simultaneous imaging of neurotransmitter inputs and neuronal activity.

Limitations of the Study

Here, we identified the relationship between glutamate input and the Ca^{2+} response. In the *eat-4* mutants, however, the Ca^{2+} responses were rare but were not completely abolished. We acknowledge that other neurotransmitters, such as neuropeptides, also affect the Ca^{2+} response in AIY (Aoki et al., 2017; Kuhara et al., 2011; Rabinowitch et al., 2016). Although our results show that decreases in glutamate evoke Ca^{2+} responses in AIY under natural noise, cooperation between several neurotransmitters could modulate the responsiveness of AIY to glutamate inputs, which would modulate sensory information and the behavioral response.

In this study, we revealed the relationships with and without odor condition. However, it is difficult to generalize for the other sensory stimulation, and modulation of the other environmental modalities could have yielded different results. In addition to the different neurotransmitters involved, AIY neurons receive glutamate from several types of sensory neurons (Clark et al., 2006; Kuhara et al., 2011; Kunitomo et al., 2013; Serrano-Saiz et al., 2013; Wang et al., 2017; White et al., 1986). For example, high concentration of

salt affects odor sensory neurons (Leinwand and Chalasani, 2013). So, the other sensory stimulation could change the input-output relationship in AIY.

We showed that mutation of *glc-3* and *eat-4* reduced the frequency of Ca^{2+} spikes. Because GLC-3 is a glutamate-gated chloride channel (Horoszok et al., 2001), ablation of the glutamate signal should depolarize the membrane potential of AIY neurons. However, shapes of Ca^{2+} spikes were identical (Figure S2). This indicates that AIY neurons retain the function of Ca^{2+} spike generation even without glutamate inputs. This suggests that the AIY neurons should have maintained their equilibrium potential even in the mutant animals because depolarization is necessary for generating Ca^{2+} spikes (Liu et al., 2018; Shindou et al., 2019). In the mutants, glutamate inputs could not cause the depolarization of membrane potential beyond the threshold in response to environmental fluctuations by glutamate inputs, so the Ca^{2+} spike frequency decreased. However, the mutations could change the physiological property in AIY; we could not dismiss these effects in the mutants.

We also noted that *C. elegans* does not have voltage-gated Na^{+} channels in its neurons (Faumont et al., 2011, 2006; Gao and Zhen, 2011; Goodman et al., 1998; Mellem et al., 2008; Shidara et al., 2013). This fact indicates that the mechanism of spike generation should be different from that of the other animals. Therefore, it is difficult to directly extrapolate our conclusions beyond *C. elegans*.

METHODS

All methods can be found in the accompanying Transparent Methods supplemental file.

SUPPLEMENTAL INFORMATION

Supplemental Information can be found online at https://doi.org/10.1016/j.isci.2019.07.028.

ACKNOWLEDGMENTS

Some plasmids for expression for the indicators were provided by a Grant-in-Aid for Scientific Research on Innovative Areas (Comprehensive Brain Science Network) from the Ministry of Education, Science, Sports and Culture of Japan. We would like to thank Prof. Loren Looger and HHMI Janelia Farm for providing iGluSnFR plasmids. N2, *glc-3*, and *eat-4* mutant strains were provided by the Caenorhabditis Genetics Center (CGC), which is funded by NIH Office of Research Infrastructure Programs (P40 OD010440). We would like to thank Prof. Cornelia I Bargmann at the Rockefeller University for providing strain and plasmid for unc-122::dsRed.

AUTHOR CONTRIBUTIONS

K.A. designed the research. K.A. performed all experiments and analysis. K.A. wrote the first draft of the manuscript. K.A., K.O., and K. H. edited the manuscript. K.A., K.O., and K. H. contributed to data interpretation. K.O. and K. H. supervised the research.

DECLARATION OF INTERESTS

The authors declare no competing interests.

Received: April 8, 2019
Revised: June 21, 2019
Accepted: July 18, 2019
Published: September 27, 2019

REFERENCES

Aoki, I., Nakano, S., and Mori, I. (2017). Molecular mechanisms of learning in Caenorhabditis elegans. In Learning and Memory: A Comprehensive Reference, J. Byrne, ed. (Elsevier), pp. 415–434.

Augustine, G.J., Santamaria, F., and Tanaka, K. (2003). Local calcium signaling in neurons. Neuron *40*, 331–346.

Branco, T., and Häusser, M. (2010). The single dendritic branch as a fundamental functional unit in the nervous system. Curr. Opin. Neurobiol. *20*, 494–502.

Callaway, E.M., and Katz, L.C. (1993). Photostimulation using caged glutamate reveals functional circuitry in living brain slices. Proc. Natl. Acad. Sci. U S A *90*, 7661–7665.

Chalasani, S.H., Chronis, N., Tsunozaki, M., Gray, J.M., Ramot, D., Goodman, M.B., and Bargmann, C.I. (2007). Dissecting a circuit for olfactory behaviour in *Caenorhabditis elegans*. Nature *450*, 63–70.

Cichon, J., and Gan, W.-B. (2015). Branch-specific dendritic Ca^{2+} spikes cause persistent synaptic plasticity. Nature *520*, 180–185.

Clark, D.A., Biron, D., Sengupta, P., and Samuel, A.D.T. (2006). The AFD sensory neurons encode multiple functions underlying thermotactic behavior in *Caenorhabditis elegans*. J. Neurosci. *26*, 7444–7451.

Destexhe, A. (2011). Intracellular and computational evidence for a dominant role of internal network activity in cortical computations. Curr. Opin. Neurobiol. *21*, 717–725.

Faisal, A.A., Selen, L.P.J., and Wolpert, D.M. (2008). Noise in the nervous system. Nat. Rev. Neurosci. *9*, 292–303.

Faumont, S., Boulin, T., Hobert, O., and Lockery, S.R. (2006). Developmental regulation of whole cell capacitance and membrane current in identified interneurons in *C. elegans*. J. Neurophysiol. *95*, 3665–3673.

Faumont, S., Lindsay, T., and Lockery, S. (2012). Neuronal microcircuits for decision making in *C. elegans*. Curr. Opin. Neurobiol. *22*, 580–591.

Faumont, S., Rondeau, G., Thiele, T.R., Lawton, K.J., McCormick, K.E., Sottile, M., Griesbeck, O., Heckscher, E.S., Roberts, W.M., Doe, C.Q., and Lockery, S.R. (2011). An image-free opto-mechanical system for creating virtual environments and imaging neuronal activity in freely moving *Caenorhabditis elegans*. PLoS One *6*, e24666.

Frick, A., Magee, J., and Johnston, D. (2004). LTP is accompanied by an enhanced local excitability of pyramidal neuron dendrites. Nat. Neurosci. *7*, 126–135.

Gao, S., and Zhen, M. (2011). Action potentials drive body wall muscle contractions in *Caenorhabditis elegans*. Proc. Natl. Acad. Sci. U S A *108*, 2557–2562.

Goodman, M.B., Hall, D.H., Avery, L., and Lockery, S.R. (1998). Active currents regulate sensitivity and dynamic range in *C. elegans* neurons. Neuron *20*, 763–772.

Horoszok, L., Raymond, V., Sattelle, D.B., and Wolstenholme, A.J. (2001). GLC-3: a novel fipronil and BIDN-sensitive, but picrotoxinin-insensitive, L-glutamate-gated chloride channel subunit from *Caenorhabditis elegans*. Br. J. Pharmacol. *132*, 1247–1254.

Jeong, H., and Paik, Y.-K. (2017). MGL-1 on AIY neurons translates starvation to reproductive plasticity via neuropeptide signaling in *Caenorhabditis elegans*. Dev. Biol. *430*, 80–89.

Jin, L., Han, Z., Platisa, J., Wooltorton, J.R.A., Cohen, L.B., and Pieribone, V.A. (2012). Single action potentials and subthreshold electrical events imaged in neurons with a fluorescent protein voltage probe. Neuron *75*, 779–785.

Kang, C., and Avery, L. (2009). Systemic regulation of starvation response in *Caenorhabditis elegans*. Genes Dev. *23*, 12–17.

Kato, S., Xu, Y., Cho, C.E., Abbott, L.F., and Bargmann, C.I. (2014). Temporal responses of *C. elegans* chemosensory neurons are preserved in behavioral dynamics. Neuron *81*, 616–628.

Kerr, R.A., and Schafer, W.R. (2006). Intracellular Ca^{2+} imaging in *C. elegans*. Methods Mol. Biol. *351*, 253–264.

Kocabas, A., Shen, C.-H., Guo, Z.V., and Ramanathan, S. (2012). Controlling interneuron activity in *Caenorhabditis elegans* to evoke chemotactic behaviour. Nature *490*, 273–277.

Kramer, R.H., Mourot, A., and Adesnik, H. (2013). Optogenetic pharmacology for control of native neuronal signaling proteins. Nat. Neurosci. *16*, 816–823.

Kuhara, A., Ohnishi, N., Shimowada, T., and Mori, I. (2011). Neural coding in a single sensory neuron controlling opposite seeking behaviours in *Caenorhabditis elegans*. Nat. Commun. *2*, 355.

Kunitomo, H., Sato, H., Iwata, R., Satoh, Y., Ohno, H., Yamada, K., and Iino, Y. (2013). Concentration memory-dependent synaptic plasticity of a taste circuit regulates salt concentration chemotaxis in *Caenorhabditis elegans*. Nat. Commun. *4*, 2210.

Lee, R.Y., Sawin, E.R., Chalfie, M., Horvitz, H.R., and Avery, L. (1999). EAT-4, a homolog of a mammalian sodium-dependent inorganic phosphate cotransporter, is necessary for glutamatergic neurotransmission in *Caenorhabditis elegans*. J. Neurosci. *19*, 159–167.

Leinwand, S.G., and Chalasani, S.H. (2013). Neuropeptide signaling remodels chemosensory circuit composition in *Caenorhabditis elegans*. Nat. Neurosci. *16*, 1461–1467.

Li, Z., Liu, J., Zheng, M., and Xu, X.Z.S. (2014). Encoding of both analog- and digital-like behavioral outputs by one *C. elegans* interneuron. Cell *159*, 751–765.

Liu, Q., Hollopeter, G., and Jorgensen, E.M. (2009). Graded synaptic transmission at the *Caenorhabditis elegans* neuromuscular junction. Proc. Natl. Acad. Sci. U S A *106*, 10823–10828.

Liu, Q., Kidd, P.B., Dobosiewicz, M., and Bargmann, C.I. (2018). *C. elegans* AWA olfactory neurons fire calcium-mediated all-or-none action potentials. Cell *175*, 57–70.e17.

Losonczy, A., Makara, J.K., and Magee, J.C. (2008). Compartmentalized dendritic plasticity and input feature storage in neurons. Nature *452*, 436–441.

Marvin, J.S., Borghuis, B.G., Tian, L., Cichon, J., Harnett, M.T., Akerboom, J., Gordus, A., Renninger, S.L., Chen, T.-W., Bargmann, C.I., et al. (2013). An optimized fluorescent probe for visualizing glutamate neurotransmission. Nat. Methods *10*, 162–170.

Mellem, J.E., Brockie, P.J., Madsen, D.M., and Maricq, A.V. (2008). Action potentials contribute to neuronal signaling in *C. elegans*. Nat. Neurosci. *11*, 865–867.

Nienborg, H., and Cumming, B.G. (2009). Decision-related activity in sensory neurons reflects more than a neuron's causal effect. Nature *459*, 89–92.

Ogawa, H., and Oka, K. (2015). Direction-specific adaptation in neuronal and behavioral responses of an insect mechanosensory system. J. Neurosci. *35*, 11644–11655.

Ohnishi, N., Kuhara, A., Nakamura, F., Okochi, Y., and Mori, I. (2011). Bidirectional regulation of thermotaxis by glutamate transmissions in *Caenorhabditis elegans*. EMBO J. *30*, 1376–1388.

Prešern, J., Triblehorn, J.D., and Schul, J. (2015). Dynamic dendritic compartmentalization underlies stimulus-specific adaptation in an insect neuron. J. Neurophysiol. *113*, 3787–3797.

Rabinowitch, I., Laurent, P., Zhao, B., Walker, D., Beets, I., Schoofs, L., Bai, J., Schafer, W.R., and Treinin, M. (2016). Neuropeptide-driven cross-modal plasticity following sensory loss in *Caenorhabditis elegans*. PLoS Biol. *14*, e1002348.

Renart, A., and Machens, C.K. (2014). Variability in neural activity and behavior. Curr. Opin. Neurobiol. *25*, 211–220.

Satoh, Y., Sato, H., Kunitomo, H., Fei, X., Hashimoto, K., and Iino, Y. (2014). Regulation of experience-dependent bidirectional chemotaxis by a neural circuit switch in *Caenorhabditis elegans*. J. Neurosci. *34*, 15631–15637.

Serrano-Saiz, E., Poole, R.J., Felton, T., Zhang, F., De La Cruz, E.D., and Hobert, O. (2013). Modular control of glutamatergic neuronal identity in *C. elegans* by distinct homeodomain proteins. Cell *155*, 659–673.

Shidara, H., Hotta, K., and Oka, K. (2017). Compartmentalized cGMP responses of olfactory sensory neurons in *Caenorhabditis elegans*. J. Neurosci. *37*, 3753–3763.

Shidara, H., Kobayashi, J., Tanamoto, R., Hotta, K., and Oka, K. (2013). Odorant-induced membrane potential depolarization of AIY interneuron in *Caenorhabditis elegans*. Neurosci. Lett. *541*, 199–203.

Shindou, T., Ochi-Shindou, M., Murayama, T., Saita, E., Momohara, Y., Wickens, J.R., and Maruyama, I.N. (2019). Active propagation of dendritic electrical signals in *C. elegans*. Sci. Rep. *9*, 3430.

Stuart, G.J., and Spruston, N. (2015). Dendritic integration: 60 years of progress. Nat. Neurosci. *18*, 1713–1721.

Tsukada, Y., Yamao, M., Naoki, H., Shimowada, T., Ohnishi, N., Kuhara, A., Ishii, S., and Mori, I. (2016). Reconstruction of spatial thermal gradient encoded in thermosensory neuron AFD in *Caenorhabditis elegans*. J. Neurosci. *36*, 2571–2581.

Ventimiglia, D., and Bargmann, C.I. (2017). Diverse modes of synaptic signaling, regulation, and plasticity distinguish two classes of *C. elegans* glutamatergic neurons. Elife *6*. https://doi.org/10.7554/eLife.31234.

Wang, L., Sato, H., Satoh, Y., Tomioka, M., Kunitomo, H., and Iino, Y. (2017). A gustatory neural circuit of *Caenorhabditis elegans* generates memory-dependent behaviors in Na^+ chemotaxis. J. Neurosci. *37*, 2097–2111.

White, J.G., Southgate, E., Thomson, J.N., and Brenner, S. (1986). The structure of the nervous system of the nematode *Caenorhabditis elegans*. Philos. Trans. R. Soc. B Biol. Sci. *314*, 1–340.

Yoshida, K., Hirotsu, T., Tagawa, T., Oda, S., Wakabayashi, T., Iino, Y., and Ishihara, T. (2012). Odour concentration-dependent olfactory preference change in *C. elegans*. Nat. Commun. *3*, 739.

Zhao, Y., Araki, S., Wu, J., Teramoto, T., Chang, Y.-F., Nakano, M., Abdelfattah, A.S., Fujiwara, M., Ishihara, T., Nagai, T., and Campbell, R.E. (2011). An expanded palette of genetically encoded Ca^{2+} indicators. Science *333*, 1888–1891.

ISCI, Volume *19*

Supplemental Information

The Input-Output Relationship of AIY Interneurons in *Caenorhabditis elegans* in Noisy Environment

Keita Ashida, Kohji Hotta, and Kotaro Oka

Supplemental Information
Transparent methods
C. elegans strains

Worms were cultured at 20°C on nematode growth medium agar plates with *Escherichia coli* OP50 bacteria under standard conditions (Brenner, 1974). Hermaphrodites were used for all experiments. The following transgenic strains were created via microinjection into the Bristol strain N2 (wild type), RB594 *glc-3* (ok321) V, and MT6308 *eat-4* (ky5) III. The transgenic strains used for this research were as follows: *okaEx5[pttx-3::iGluSnFR, 50 ng/μL + pttx-3::R-GECO1, 50 ng/μL]*, *okaEx6[pttx-3::ArcLight, 50 ng/μL + pttx-3::R-GECO1, 50 ng/μL]*, *okaEx10[pttx-3::GCaMP6, 50 ng/μL + pttx-3::dimer2, 50 ng/μL], okaEx15; glc-3 (ok321) X [pttx-3::iGluSnFR, 50 ng/μL + pttx-3::R-GECO1, 40 ng/μL + punc-122::dsRed, 15 ng/μL]*, and *okaEx16; eat-4 (ky5) X [pttx-3::iGluSnFR, 50 ng/μL + pttx-3::R-GECO1, 40 ng/μL + punc-122::dsRed 15 ng/μL]*.

Plasmids

For ArcLight expression, codon-optimized ArcLight was synthesized using *C. elegans* Codon Adapter (Redemann et al., 2011) (Integrated DNA Technologies Genes). This codon-optimized ArcLight was cloned into a Gateway Destination vector (Thermo Fisher Scientific). Gateway Destination vectors for expressing proteins and Gateway Entry vectors (Thermo Fisher Scientific) for cell-specific promoters were obtained from the Comprehensive Brain Science Network. All plasmids used to express proteins in the animals were generated from these vectors using Gateway Cloning Technology (Thermo Fisher Scientific).

Confocal imaging

Confocal images of detailed neuronal structures (Figures 1A and 2A) were acquired using a confocal laser scanning microscopy system (FluoView FV1000, Olympus) mounted on an inverted microscope (IX81, Olympus) using a 40× objective oil-immersion lens (UPLFLN 40XO, Olympus) for animals expressing ArcLight and R-GECO or iGluSnFR and R-GECO in their AIY neurons. Animals were immobilized with 20 mM sodium azide and mounted in a 1% low-melting-point agarose gel (UltraPure, Invitrogen). The imaging conditions were excitation at 488 nm and detection at 500–545 nm for ArcLight and iGluSnFR, and excitation at 559 nm and detection at 570–670 nm for R-GECO.

Ca^{2+}, glutamate and voltage imaging

We used a genetically encoded Ca^{2+} indicator, R-GECO1 (Zhao et al., 2011), a genetically encoded Ca^{2+} indicator, G-CaMP6 (Ohkura et al., 2012) with dimer 2 (Campbell et al., 2002) (RFP as a reference), a genetically encoded glutamate indicator, iGluSnFR (Marvin et al., 2013), and a genetically encoded voltage indicator, ArcLight (Jin et al., 2012) with olfactory chips (Chronis et al., 2007). The olfactory chips are microfluidic devices that can control stimulation temporally via valve switching. The animals were stimulated with S-basal buffer and isoamyl alcohol (IAA) diluted with S-basal buffer (9.2×10^{-4} mol/L). For Ca^{2+} and glutamate imaging, the animals were stimulated with 60 s S-basal buffer, 60 s diluted IAA, and again 60 s S-basal buffer (as shown in Figure 3B). To simultaneously image Ca^{2+} and membrane potential under odor stimulation, images were acquired over 70 s immediately after switching from S-basal to diluted IAA. For the no-odor condition, images were acquired without changing the buffer. To reduce the effects of photobleaching, we used images taken after 60 s for analysis. Images were acquired every 100 ms for Ca^{2+} and glutamate imaging, and every 20 ms for Ca^{2+} and membrane potential imaging; the exposure time was equal to the interval duration (100 or 20 ms) in each case. We used an inverted microscope (IX71, Olympus) with a LED light source (SOLA, Lumencor), and a 3CCD camera (C7800-20, Hamamatsu Photonics). Images were acquired using an AQUACOSMOS (Hamamatsu Photonics) with a 20× objective lens (UCPLFLN 20X, Olympus) and a 1.6× zoom lens. A BrightLine GFP/DSRED-A (Semrock) cube was used. We noted that ArcLight becomes dim when the membrane potential depolarizes, while R-GECO becomes bright when Ca^{2+} increases. The membrane potential spikes in Figures 1B and 1C are thus not artifacts of fluorescent leakage by R-GECO. In addition, photobleaching causes an increase of the ArcLight traces in Figure 1B because we showed $-\Delta F/F_0$ for the ArcLight traces. To reduce noise caused by movement of the animals, a cholinergic agonist, levamisole (2 mM), was used in the S-basal buffer. In preliminary experiments, we demonstrated that levamisole did not affect the AIY spike frequency (Figure S1).

Image analysis

We analyzed the imaging data using the same semi-automated custom software written in MATLAB (MathWorks) that we used in a previous study (Shidara et al., 2017). Regions

of interest were determined based on fluorescence intensities and the morphology of the neurons (Figures 1A and 2A). We measured the Ca^{2+} response and glutamate input at the AIY neurite, because these interneurons show a clear Ca^{2+} response at the neurite but not at the soma (Chalasani et al., 2007; Clark et al., 2006). All fluorescence intensity data were normalized by the average intensities for the first 2 s, and are presented as ΔF/F.

Data analysis and statistical tests

Statistical tests were performed in Excel 2011 (paired t-test and Welch's t-test, using the "TTEST" function), Python 3 (version: 3.7.0; tests for Pearson correlation coefficients were conducted using the "stats.pearsonr" function in the SciPy library (version 1.1.0)), and R (version: 3.4.3; Wilcoxon signed rank tests were conducted using the "wilcoxsign_test" function with the "exact" option, and Wilcoxon rank sum tests were conducted using the "wilcox_test" function with the "exact" option in the coin package).

The average intensities of the Ca^{2+} and membrane potential spikes in Figure 1C were generated by detecting Ca^{2+} spikes as described below. The peak values of membrane potential in Figures 1D and 1E were calculated by subtracting the average values for the 1 s period from −1 s to −2 s in Figure 1C from the maximal values for the 1 s period from −1 s to 0 s. The Ca^{2+} increases were calculated by subtracting the average intensities for the 1 s period from −1 s to 0 s from the maximal intensities for the 1 s period from 0.5 s to 1.5 s.

The averaged intensities over the 20 s before and after odor addition are shown in Figure 2C (left), and the average intensities over the 20 s before and after odor removal are shown in Figure 2C (right).

We classified the odor stimulation conditions into two groups, early odor and later odor, for Figures 3–6. The early odor condition comprised the data from the first 10 s after the onset of odor stimulation, and the later odor condition comprised the data from 10–60 s after odor addition (see Figure 3B). Odor addition reduced glutamate-input levels immediately (Figure 2B), so we considered two conditions to be transient and stable, respectively.

We classified the data based on whether Ca^{2+} spikes were present or absent (with or without) for Figures 3, 5, and 6. The Ca^{2+} spikes in Figure 3C were extracted as described below, and data that did not include Ca^{2+} spikes were considered non-Ca^{2+}

spiking data. All glutamate responses were normalized to zero at time 0. The intensities before the Ca^{2+} spike ("pre" in Figure 3D) are the average intensities for the 1 s period from −3 s to −2 s in Figure 3C, and the average intensities during the spike ("onset" in Figure 3D) are the average intensities for the 1 s period from −0.5 s to +0.5 s in Figure 3C. The glutamate decreases in Figure 3E and 3F were calculated by subtracting the "onset" intensities in Figure 3D from the "pre" intensities. The Ca^{2+} increases in Figure 3E were calculated by subtracting the average intensities for the 1 s period from −1 s to 0 s (as in Figure 3C) from the average intensities for the 1 s period from 2 s to 3 s.

The Ca^{2+} responses to glutamate decreases, shown in Figure 4A were collected as described below. All Ca^{2+} responses were normalized to zero at time 0. The intensities before and during the response in Figure 4B were calculated as for Figure 3D. The randomly selected data in Figures 4C and 4D are described below. The Ca^{2+} increases shown in Figure 4D were calculated by subtracting the average intensities before the response ("pre" in Figure 4B) from those during the response ("onset" in Figure 4B).

The average intensities of the glutamate input shown in Figure 5B were calculated as for Figure 2C; Figures 5C–5E were generated in the same manner as Figures 3C, 3D, and 3F.

The average intensities of glutamate input shown in Figure 6B were calculated as for Figure 2C. The probability of a Ca^{2+} spike in response to odor stimulation shown in Figure 6C was calculated by counting the Ca^{2+} spikes during the early-odor period. The frequency of the Ca^{2+} spikes in Figure 6D was calculated by counting the Ca^{2+} spikes detected as described below. Figures 6E–6G were generated in the same manner as Figures 3C, 3D, and 3F.

Extracting Ca^{2+} spikes and glutamate decreases

To extract the Ca^{2+} spikes, we selected a data point at near the beginning of the Ca^{2+} data, and calculated the difference between the average intensities for the 5 s period before and after before that point. If the difference was larger than the average intensity over the 5 s period before the point plus three standard deviations, the point was determined to be the onset of a Ca^{2+} spike, after visual verification. To extract the glutamate-decrease point shown in Figure 4, we selected a data point at near the beginning of the glutamate data and calculated the difference between the averaged intensities for the 5 s period before and after that point. If the difference was larger than the threshold (0.025; determined

from the values in Figure 3F), the point was automatically determined to be the onset of a glutamate decrease. For Ca^{2+} and glutamate decreases, we collected the data for 5 s periods before and after the points that had been detected as described above. There was no overlap between the collected data. Finally, we defined all data that did not include a Ca^{2+} spike as the data without a Ca^{2+} spike.

In Figure S1, we counted the Ca^{2+} spikes manually, because the signal-to-noise ratio differed between the with- and without-levamisole conditions. We counted the spikes from 70 s to 120 s for Figure S1B, and from 60 s to 70 s for Figure S1C.

Random resampling

Randomly resampled data are used in Figures 4C and 4D. One hundred time points were selected randomly using the "randint" function (in Python numpy.random in NumPy library (version 1.15.2)), and we extracted 10 s of data after each of these points. We initialized the seed of the random number generator using the current system time.

Supplemental figures

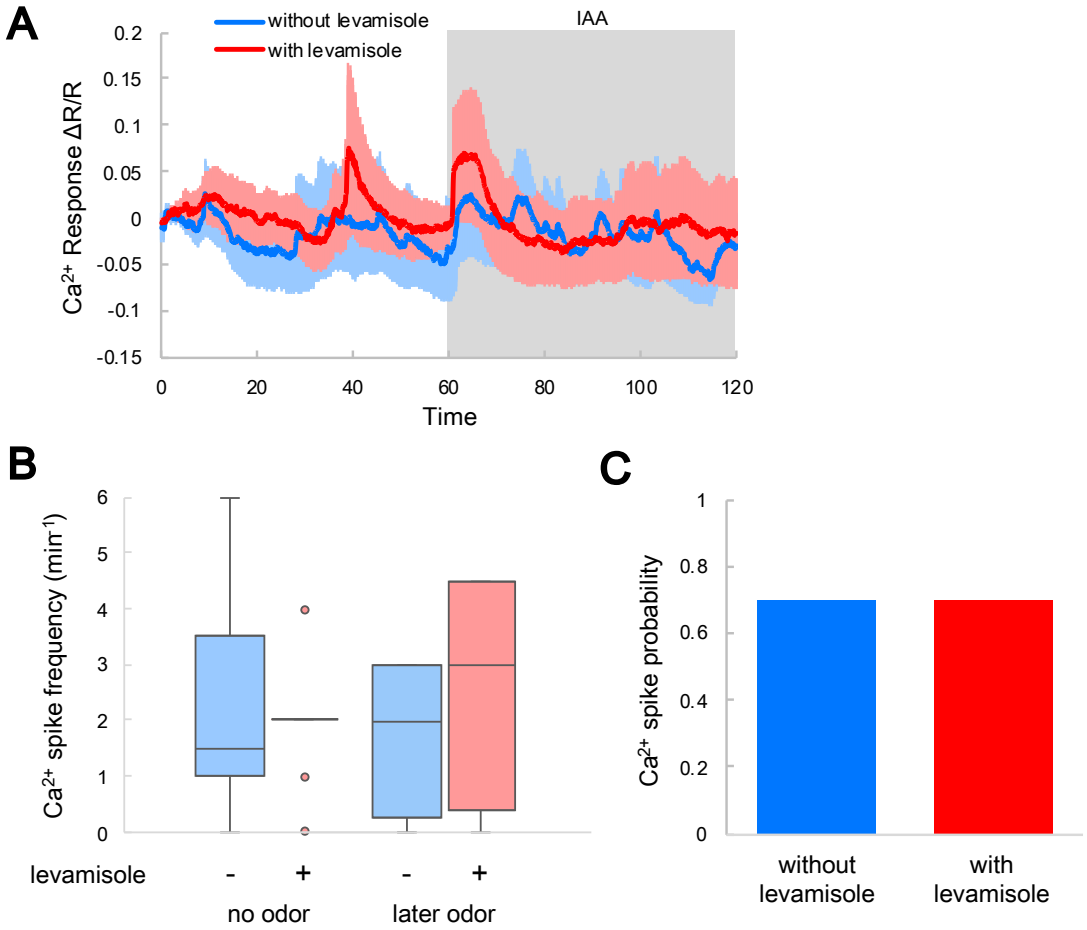

Figure S1. Levamisole does not significantly affect Ca^{2+} spikes in AIY. Related to Figure 1.

(A) The Ca^{2+} response in AIY to odor with (red) and without (blue) levamisole. The shaded region is odor stimulation.

(B) Spike frequency without (from 0 s to 60 s) and with (from 70 s to 120 s) odor stimulation, with (red) and without (blue) levamisole. Box plots indicate the median (center line), quartiles (boxes), and range (whiskers). The statistical metrics are as follows: no odor, p = 0.75, later odor, p = 0.80. Wilcoxon rank sum test (without levamisole, N = 10; with levamisole, N = 10).

(C) Ca^{2+} spike probability immediately after odor stimulation with and without levamisole. The statistical metrics are as follows; p = 1.0, Fisher's exact test (without levamisole, N = 10; with levamisole, N = 10).

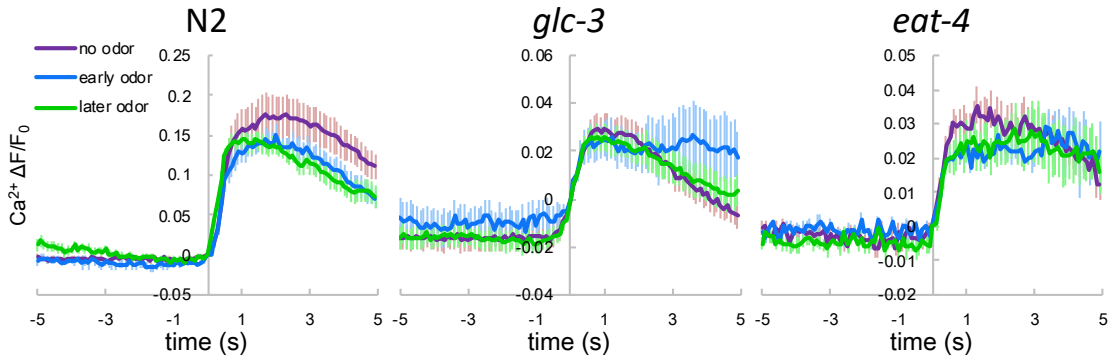

Figure S2. Averaged Ca^{2+} responses. Related to Figures 3, 5 and 6.

Time 0 indicates the onset of Ca^{2+} spikes. All Ca^{2+} responses were normalized to zero at time 0. The purple, blue and green lines indicate the responses under the no-odor, early-odor, and later-odor conditions, respectively. Shadows indicate the SEM (N2: N = 15; no odor, n = 15; early odor, n = 11; later odor, n = 20; *glc-3*: N = 12, no odor, n = 15; early odor, n = 6; later odor, n = 20; *eat-4*: N = 12, no odor: n = 9; early odor, n = 3; later odor, n = 9).